

Tunable Intrinsic Plasmons due to Band Inversion in Topological Materials

Furu Zhang,¹ Jianhui Zhou,^{2,3,*} Di Xiao,² and Yugui Yao^{1,†}

¹*Beijing Key Laboratory of Nanophotonics and Ultrafine Optoelectronic Systems,
School of Physics, Beijing Institute of Technology, Beijing 100081, China*

²*Department of Physics, Carnegie Mellon University, Pittsburgh, Pennsylvania 15213, USA*

³*Department of Physics, The University of Hong Kong, Pokfulam Road, Hong Kong, China*

The band inversion has led to rich physical effects in both topological insulators and topological semimetals. It has been found that the inverted band structure with the Mexican-hat dispersion could enhance the interband correlation leading to a strong intrinsic plasmon excitation. Its frequency ranges from several meV to tens of meV and can be effectively tuned by the external fields. The electron-hole asymmetric term splits the peak of the plasmon excitation into double peaks. The fate and properties of this plasmon excitation can also act as a probe to characterize the topological phases even in the lightly doped systems. We numerically demonstrate the impact of the band inversion on plasmon excitations in magnetically doped thin films of three-dimensional strong topological insulators, V- or Cr-doped (Bi,Sb)₂Te₃, which support the quantum anomalous Hall states. Our work thus sheds some new light on the potential applications of topological materials in plasmonics.

Introduction.—Plasmons are ubiquitous collective density oscillations of an electron liquid and can occur in metals, doped semiconductors and semimetals [1, 2]. The frequency of plasmon excitation is usually proportional to the density of states (DOS) of carriers at the Fermi level in the long wavelength limit [3]. In systems with vanishing DOS at the Fermi level, however, it had been demonstrated that strong correlation, higher order term in the effective mass, and the chiral anomaly could give rise to exotic plasmon excitations at zero temperature in the context of two dimensional (2D) Anderson insulators [4], graphene [5], HgTe quantum well [6], and three-dimensional (3D) Weyl semimetals [7], respectively. In this paper, we reveal a new mechanism based on the band inversion with the Mexican-hat dispersion that can be used to excite and manipulate intrinsic plasmon excitations in topological materials even with vanishing DOS.

The band inversion has played a critical role in the transport properties of both topological insulators and topological semimetals, which have attracted intensive interest in condensed matter physics [8–11]. However, there has been little study of the effect of band inversion on the optical properties of topological materials [12]. Recently, the experimental observation of the quantum anomalous Hall (QAH) effect [13, 14] has been reported in magnetically doped ultrathin films of topological insulators V- or Cr-doped (Bi, Sb)₂Te₃ [15–17], in which its band topology can be tuned by external fields. On the other hand, some recent experimental efforts have been made on observing the plasmon excitations in the bulk or surface of both the magnetic and nonmagnetic 3D topological insulators [18–26]. The frequency of these plasmon excitations ranges from terahertz to far infrared and facilitates a wide variety of applications of topological insulators, such as in information and communication, chemical and biological sensing, and medical sciences [27–29]. Therefore, these QAH topological materials provide us with a promising platform to controllably create and

manipulate collective excitations via the band inversion mechanism, a new control knob for the field of plasmonics [1].

In this paper, we show that the inverted band structure with the Mexican-hat dispersion could enhance the interband correlation, leading to a strong intrinsic plasmon excitation. We theoretically examine the relevant physics in both the intrinsic and lightly doped thin films of topological insulators. The frequency of the resulting intrinsic plasmon can be effectively tuned by the external fields. The peak of plasmon excitation is split into double peaks by the electron-hole asymmetry. Consequently, the plasmon excitation provides us with an effective tool to identify the topological phases.

Model of the QAH systems.—To demonstrate our theory, we begin with the following Hamiltonian that describes the band inversion in the magnetically doped thin films of topological insulators V- or Cr-doped (Bi, Sb)₂Te₃ [30]

$$H = H_0 + \frac{m}{2}\tau_0 \otimes \sigma_z, \quad (1)$$

where m is the exchange field originating from the magnetic dopants, effectively acting as a Zeeman field. H_0 is given by [31, 32]

$$H_0 = -Dk^2 + \begin{pmatrix} h_+(\mathbf{k}) & V \\ V & h_-(\mathbf{k}) \end{pmatrix}, \quad (2)$$

with

$$h_{\pm}(\mathbf{k}) = \begin{pmatrix} \pm(\frac{\Delta}{2} - Bk^2) & iv_F k_- \\ -iv_F k_+ & \mp(\frac{\Delta}{2} - Bk^2) \end{pmatrix},$$

where $h_{\pm}(\mathbf{k})$ describes the 2D Dirac fermions with a \mathbf{k} -dependent mass. Here $\mathbf{k} = (k_x, k_y)$ is the 2D wave vector, $k_{\pm} = k_x \pm ik_y$ and $k = \sqrt{k_x^2 + k_y^2}$, v_F is the effective velocity, the D term breaks the electron-hole symmetry, Δ is the hybridization of the top and bottom surface states

of the thin film, and V measures the structural inversion asymmetry between the top and bottom surfaces. The Pauli matrices τ_0 and σ_z act on the pseudospin space related to the top and bottom surfaces and the real spin degree of freedom, respectively. In this paper we primarily consider the insulating phase that requires $|D| < |B|$. The actual value of the parameters describes realistic materials [14, 15]. Specifically, $v_F = 3.0 \text{ eV} \cdot \text{\AA}$, $V = 0.03 \text{ eV}$ and $B = -30 \text{ eV} \cdot \text{\AA}^2$.

Let us first discuss the topological properties of the Hamiltonian in Eq. (1). As the exchanged field m increases, the system will undergo a topological phase transition from a trivial phase to a nontrivial one or vice versa. The critical value of the exchanged field is $m_0 = -\sqrt{\Delta^2 + 4V^2}$. It is useful to introduce a dimensionless parameter $\xi = m/m_0$ to mark the topological phase transition. When $\xi < 1$, the system is in a topologically trivial phase, and when $\xi > 1$, it is in a nontrivial phase with chiral edge states [15]. The band gap between the two inner bands closes at the critical point with $\xi = 1$. Fig. 1(a) clearly exhibits that in the trivial phase, the band edge have an obvious Mexican-hat like inverted band structure. The joint density of states near the band edge of this inverted band exhibits a 1D behavior and possesses a Van Hove singularity at a finite wave vector, in which the corresponding DOS diverges, as shown in Fig. 1(c). On the other hand, in the nontrivial phase [see Fig. 1(b)], all the four bands are parabolic, i.e., uninverted [30]. The DOS near these band edges does not possess a strong singularity [Fig. 1(d)]. In addition, Figs. 1(e)-1(f) show a great enhancement of the overlap of wave functions due to the band inversion.

Band inversion mechanism for plasmons.—We start from the general dielectric function at arbitrary wave vector \mathbf{q} and frequency ω within the random phase approximation [3]

$$\varepsilon(\mathbf{q}, \omega) = 1 - V(\mathbf{q})\Pi(\mathbf{q}, \omega), \quad (3)$$

where $V(\mathbf{q}) = 2\pi e^2/\kappa q$ is the Fourier transform of the 2D Coulomb interaction, κ is the effective background dielectric constant. The noninteracting polarization function $\Pi(\mathbf{q}, \omega)$ has the form [33]

$$\Pi(\mathbf{q}, \omega) = \sum_{\lambda, \lambda'} \int \frac{d^2\mathbf{k}}{(2\pi)^2} \frac{f(E_{\lambda\mathbf{k}}) - f(E_{\lambda'\mathbf{k}'})}{\omega + E_{\lambda\mathbf{k}} - E_{\lambda'\mathbf{k}'} + i\eta} F_{\lambda\lambda'}(\mathbf{k}, \mathbf{k}'), \quad (4)$$

in which the overlap of eigenstates $F_{\lambda\lambda'}(\mathbf{k}, \mathbf{k}')$ is given by

$$F_{\lambda\lambda'}(\mathbf{k}, \mathbf{k}') = |\langle \mathbf{k}, \lambda | \lambda', \mathbf{k}' \rangle|^2, \quad (5)$$

where $|\lambda', \mathbf{k}'\rangle$ is the periodic part of the Bloch wave function with $\mathbf{k}' = \mathbf{k} + \mathbf{q}$. The band indices λ and λ' run over all relevant energy bands. η is related to the electron lifetime due to the Landau damping. $E_{\lambda\mathbf{k}}$ is the energy dispersion of the effective Hamiltonian, and $f(x) = [\exp\{\beta(x - \mu)\} + 1]^{-1}$ is the Fermi distribution

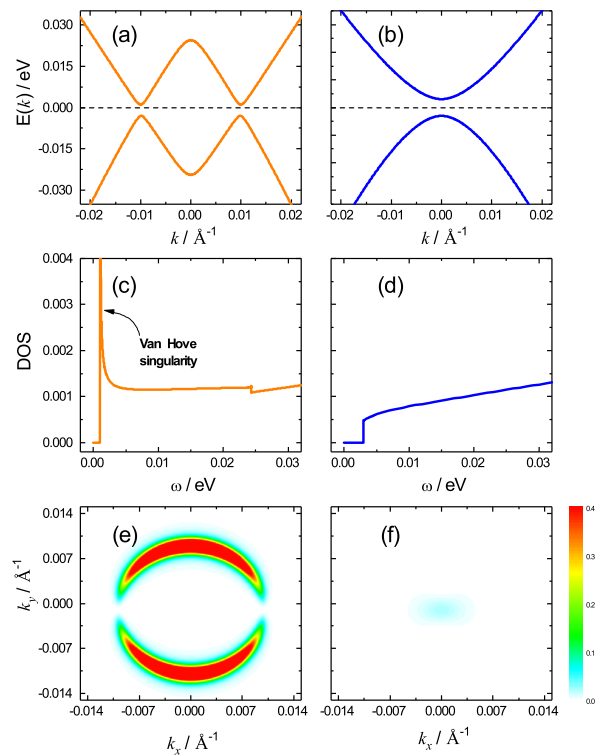


Figure 1. (color online) The band structures of the two inner bands of the thin film of topological insulators described by Eq. (1) in the trivial (a) and nontrivial (b) phases, respectively. (c) and (d) show the corresponding DOS. (e) and (f) are the intensity plots of the overlap of wave functions $F_{2,3}(\mathbf{k}, \mathbf{k}')$. Parameters: $\Delta = -0.01 \text{ eV}$, $D = 10.0 \text{ eV} \cdot \text{\AA}^2$, $\eta = 10^{-5} \text{ eV}$ and $q = 2 \times 10^{-3} \text{\AA}^{-1}$.

function with $\beta = 1/k_B T$. For simplicity, we assume zero temperature $T = 0 \text{ K}$ throughout this paper. It is well known that the plasmons can be revealed as sharp peaks in the energy-loss function, defined as the imaginary part of the inverse dielectric function [3]

$$\text{Loss}(\mathbf{q}, \omega) = \text{Im} \left[-\frac{1}{\varepsilon(\mathbf{q}, \omega)} \right], \quad (6)$$

which can be probed in various spectroscopy experiments [34], such as the electron energy-loss spectroscopy and angle-resolved photoemission spectroscopy.

The polarization function in Eq. (4) consists of both the interband and the intraband parts. When the Fermi level lies in the band gap, at zero temperature, the intraband transition is forbidden. Thus, the interband correlation will determine the plasmon excitations. In conventional semiconductors or insulators, the interband correlation decays rapidly because of small wave function overlap in Eq. (5). This is why the plasmon excitations usually occur in doped systems, in which the intraband correlation becomes nonzero and dominates over the interband correlation.

Here we notice that the band inversion could enhance

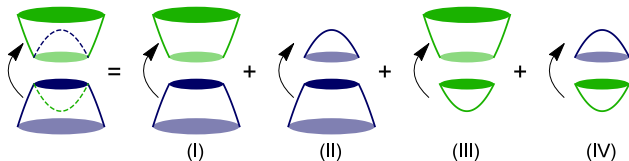


Figure 2. Schematically decomposing the interband transition between a pair of inverted bands into four distinct processes in the uninverted band picture. Processes (I) and (IV) correspond to the interband transitions, whereas processes (II) and (III) corresponding to the effective intraband transitions shall greatly enhance the interband coherence and hence are critical to the strong intrinsic plasmon excitation.

the interband correlation and give rise to a strong intrinsic plasmon excitation. To make the physics more transparent, we divide the interband transition between the two inverted bands into four different processes, as shown in Fig. 2. It is clear that the strong overlap of interband transition in the inverted band picture above corresponds to the effective intraband transition in the uninverted band picture, labeled by the processes (II) and (III) in Fig. 2. These two processes are responsible for the band-inversion enhanced interband transition due to the large wave function overlap [Figs. 1(e)-1(f)]. On the other hand, the joint DOS near the highly degenerate band minima of this inverted conduction band exhibits a 1D behavior and possesses a Van Hove singularity, in which the corresponding DOS diverges, as shown in Fig. 1(c). In addition, there exists a weak discontinuous point at the conduction band maximum in Fig. 1(c). The band-inversion induced Van Hove singularity has also played a crucial role in unconventional superconductivity [35], and ferromagnetism [36]. In the following, we show that the large interband correlation together with the Van Hove singularity is essential to give rise to strong intrinsic plasmon excitations [37].

Plasmon in intrinsic QAH systems.—To determine the plasmon dispersion in intrinsic QAH systems of thin films of V- or Cr-doped $(\text{Bi, Sb})_2\text{Te}_3$, we numerically calculate the energy loss function $\text{Loss}(\mathbf{q}, \omega)$ with several values of ξ and present the corresponding results in Figs. 3(a)-3(d). When ξ is small, the system has a clear band inversion structure [see Fig. 1(a)]. Meanwhile, there is a strong plasmon excitation in the low frequency region ($\omega < 0.05$ eV), as shown in Fig. 3(a). The plasmon dispersion scales approximately linearly with the wave vector q . The energy of this plasmon ranges from several meV to tens of meV and can be effectively tuned by external fields and other parameters. As ξ increases, the height of the peak of the Mexican hat decreases. Accordingly, the plasmons becomes weakened and their dispersion curves become short. The plasmon frequency also has an obvious red-shift due to the shrink of the gap between the two inner bands. When the topological

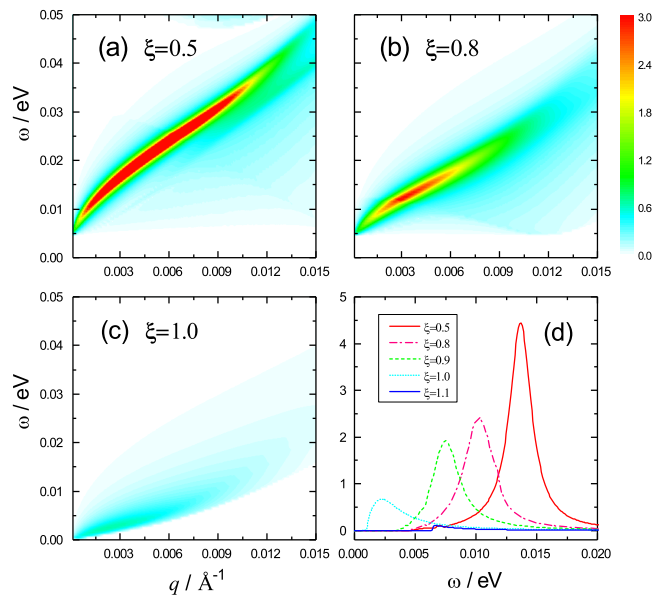


Figure 3. (color online) The evolution of the plasmon dispersion in the intrinsic QAH systems of thin films of V- or Cr-doped $(\text{Bi, Sb})_2\text{Te}_3$ for $\xi = 0.5$ (a), 0.8 (b), 1.0 (c), respectively. The color bar denotes intensities of $\text{Loss}(\mathbf{q}, \omega)$. (d) Plots of the energy-loss function at $q = 2 \times 10^{-3} \text{ \AA}^{-1}$ for different values of ξ . The effective dielectric constant is $\kappa = 5$. Other parameters are the same as those in Fig. 1.

phase transition occurs ($\xi=1$), the band gap closes, and the dispersion curve becomes shortest. Our numerical calculations also show that, after the topological phase transition ($\xi>1$), the plasmon becomes almost invisible due to the weak interband correlation. Thus, the band inversion strongly modifies the properties of this interband plasmon dispersion. It is one of the main results in this work.

The zeros in the real part of the dynamical dielectric function, $\text{Re}[\varepsilon(q, \omega)]$, can also be used to determine the plasmon excitations. Fig. 4(a) depicts the numerical results of $\text{Re}[\varepsilon(q, \omega)]$ (green line), $\text{Im}[\varepsilon(q, \omega)]$ (orange line) and the energy loss function for $\xi = 0$. It is clear that there exist two peaks (labeled by P_1 and P_2) in plasmon dispersion. The plasmon P_2 has a higher energy and a weak damping rate, which is characterized by the imaginary part of the dielectric function. Compared with P_2 , the plasmon P_1 has a lower energy and a stronger damping rate. We also note that a smaller dielectric constant κ can weaken the damping rate and thus enhance plasmon P_1 . We plot the dispersions for both plasmons in Fig. 4(b) and find that the energy split of this double peak can reach to tens of meV. Physically, plasmon P_2 (P_1) stems from the sum (difference) of processes (II) and (III) in Fig. 2. Thus, the double-peak fine structure in the plasmon dispersions is a direct consequence of the electron-hole asymmetry in Eq. (2), which breaks the degeneracy between two interband processes (II) and

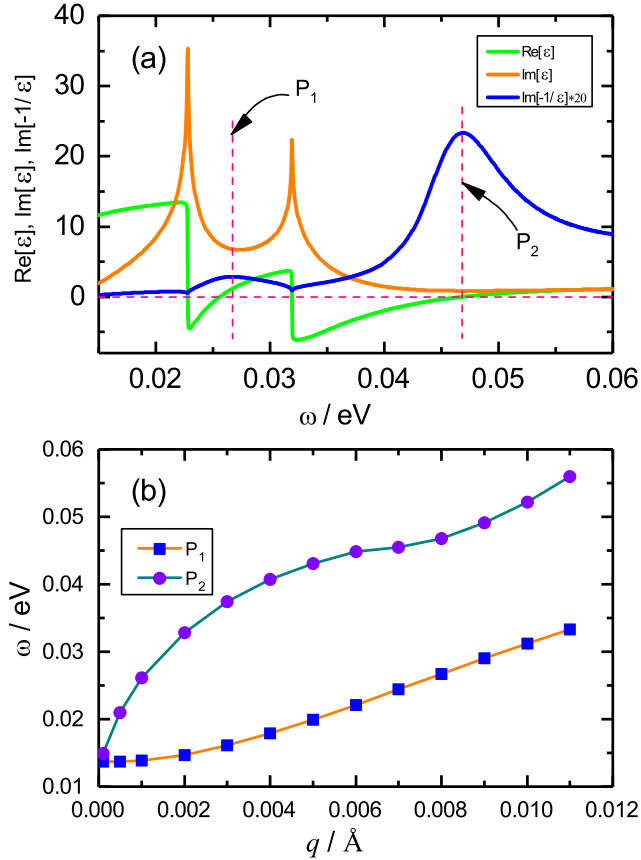


Figure 4. (color online) The double-peak structure in plasmon dispersion induced by the electron-hole asymmetric term in the thin films of V- or Cr-doped $(\text{Bi}, \text{Sb})_2\text{Te}_3$ (a). The real part, the imaginary part of the dielectric function, and the energy-loss function are labeled by the green, yellow and blue lines, respectively. (b) shows the energy dispersion of double plasmons (P_1 and P_2) determined by the peaks of the energy loss function. The parameters are $\Delta = -0.02$ eV, $D = 28$ eV \cdot \AA^2 , $\kappa = 1$, $\xi = 0$, and $q = 8 \times 10^{-3}$ \AA^{-1} .

(III) in Fig. 2. It is useful to point out that for the intrinsic gapped graphene [39, 40], silicene and other buckled honeycomb lattices [42, 43], the polarization function within the random phase approximation satisfies the relation $\text{Re}[\Pi(q, \omega)] \leq 0$ or $\text{Re}[\varepsilon(q, \omega)] \geq 1$ [39]. As a result, when the Fermi level lies in the band gap and has a vanishing DOS, these systems hardly develop a plasmon excitation at zero temperature.

Several remarks are in order here. First, this band inversion enhancement mechanism for interband plasmons is also applicable to the quantum spin Hall effect in HgTe quantum wells [8, 9], and in InAs/GaSb quantum wells [44]. Unlike the effective model in Eq. (1) we study here, the inverted bands in these systems are usually in the topologically nontrivial phase. Secondly, in Ref. [6], the dynamical polarization function and weak plasmons in HgTe quantum wells were calculated. But the mechanism to enhance and manipulate in-gap plasmon mode was not

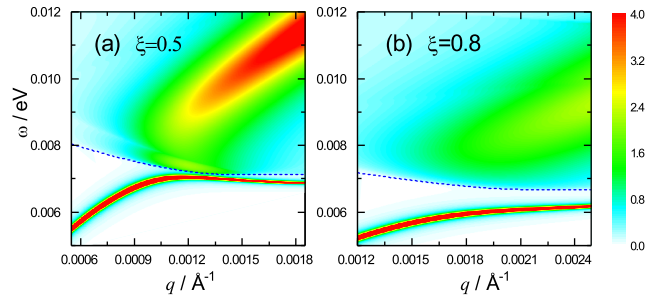


Figure 5. (color online) The energy dispersion of the plasmons for a lightly doped QAH system of a thin film of V- or Cr-doped $(\text{Bi}, \text{Sb})_2\text{Te}_3$ with $\mu = 0.004$ eV and $\kappa = 5$ for $\xi = 0.5$ (a) and 0.8 (b), respectively. The blue dashed lines determined by minima of the single particle excitation energy, guide to the eye, denote the edge of electron-hole continuum, whereas the color bar is for intensities of $\text{Loss}(\mathbf{q}, \omega)$. Other parameters are identical to those in Fig. 1.

discussed. In addition, our present work only reveals the effect of the band inversion on the longitudinal bulk plasmon excitations. The case for transverse plasmon excitations will be reported elsewhere. Note that the plasmon excitations studied here essentially differ from the edge magnetoplasmon with no magnetic fields observed in the topological nontrivial phase [25].

Plasmon in lightly doped QAH systems.—In reality, the system might be metallic due to defects, self-doping, and charge transfer from substrates, gating, etc. To gain more insights into the intrinsic plasmon excitation, we briefly discuss the impact of finite doping [45]. For the lightly doped case, the interband correlation is still strong enough to rise the novel interband plasmon, whereas a usual plasmon comes from the intraband transition. On the other hand, for the heavily doped case, the interband correlation will be significantly suppressed such that the interband plasmon excitation disappears. However, the usual intraband plasmon excitation continues to exist.

Figs. 5(a) and 5(b) depict the energy dispersion of plasmons for $\mu = 4.0$ meV measured from absolute zero. The novel interband plasmon starts from a relatively large wave vector in Fig. 5(a) and becomes weak in Fig. 5(b) and finally disappears near the topological phase transition, similar to the intrinsic case in Fig. 3. Therefore, the novel interband plasmon still exists and could signify the topological phase transition in the lightly doped QAH systems. As shown in Fig. 5(a), the usual intraband plasmon starts from a very small wave vector and shows the energy dispersion $\omega(q) \propto \sqrt{q}$ for small q , similar to the conventional 2D electron gases [2] and 2D Dirac fermions [34, 39–43]. After q exceeds 1.2×10^{-3} \AA^{-1} , its dispersion greatly deviates from \sqrt{q} . Numerical results show that the intraband plasmon survives and remains noticeable even when $\xi > 1$. Thus, this intraband plasmon is insensitive to the topology of energy bands. In

addition, the frequency of the intraband plasmon shows a continuous redshift as increasing ξ .

In summary, it has been shown that the band inversion with the Mexican-hat dispersion indeed leads to a strong intrinsic plasmon excitation with highly tunable frequencies in topological materials. The electron-hole asymmetric term could induce a double-peak fine structure in the plasmon dispersion. We have further pointed out that this intrinsic plasmon excitation can be used to characterize the topological phase transition via bulk measurements. The above physics has been numerically examined in both the intrinsic and lightly doped thin films of magnetic topological insulators V- or Cr-doped $(\text{Bi, Sb})_2\text{Te}_3$. Therefore, our work paves the way for the potential applications of topological materials in terahertz and infrared plasmonics.

A series of recent experimental advances have been made in the detection of plasmons in 3D topological insulators, in particular, in their magnetic thin films. We expect that at the current status of experimental progress, the predicted anomalous plasmons and the double-peak structure will soon be tested experimentally.

We are grateful to Hao-Ran Chang, Wen-Yu Shan and Zhi-Ming Yu for enlightening discussions. F.Z. and Y.Y. acknowledge fundings from the MOST Project of China (Nos. 2014CB920903 and 2016YFA0300603), the National Nature Science Foundation of China (Grant Nos. 11574029 and 11734003). J.Z. and D.X. were supported by AFOSR Grant No. FA9550-14-1-0277. J.Z. was also supported by the Research Grant Council, University Grants Committee, Hong Kong under Grant No. 17301116 and C6026-16W.

* jianhuizhou1@gmail.com

† ygyao@bit.edu.cn

- [1] S. Maier, *Plasmonics: Fundamentals and Applications* (Springer, New York, 2007).
- [2] G. Giuliani and G. Vignale, *Quantum theory of the electron liquid* (Cambridge University Press, Cambridge, UK, 2005).
- [3] D. Pines, *Elementary Excitations in Solids: Lectures on Protons, Electrons, and Phonons*, Vol. 5 (Westview Press, Boulder, 1999).
- [4] T. V. Shahbazyan and M. E. Raikh, *Phys. Rev. B* **53**, 7299 (1996).
- [5] S. Gangadharaiyah, A. M. Farid, and E. G. Mishchenko, *Phys. Rev. Lett.* **100**, 166802 (2008).
- [6] S. Juergens, P. Michetti, and B. Trauzettel, *Phys. Rev. Lett.* **112**, 076804 (2014).
- [7] J. Zhou, H.-R. Chang, and D. Xiao, *Phys. Rev. B* **91**, 035114 (2015).
- [8] M. Z. Hasan and C. L. Kane, *Rev. Mod. Phys.* **82**, 3045 (2010).
- [9] X.-L. Qi and S.-C. Zhang, *Rev. Mod. Phys.* **83**, 1057 (2011).
- [10] A. Bansil, H. Lin, and T. Das, *Rev. Mod. Phys.* **88**, 021004 (2016).
- [11] N. P. Armitage, E. J. Mele, and A. Vishwanath, arXiv:1705.01111 [cond-mat.str-el].
- [12] L. Z. Tan and A. M. Rappe, *Phys. Rev. Lett.* **116**, 237402 (2016).
- [13] F. D. M. Haldane, *Phys. Rev. Lett.* **61**, 2015 (1988).
- [14] R. Yu, W. Zhang, H.-J. Zhang, S.-C. Zhang, X. Dai, and Z. Fang, *Science* **329**, 61 (2010).
- [15] C.-Z. Chang, J. Zhang, X. Feng, J. Shen, Z. Zhang, M. Guo, K. Li, Y. Ou, P. Wei, L.-L. Wang, *et al.*, *Science* **340**, 167 (2013).
- [16] A. J. Bestwick, E. J. Fox, X. Kou, L. Pan, K. L. Wang, and D. Goldhaber-Gordon, *Phys. Rev. Lett.* **114**, 187201 (2015).
- [17] C.-Z. Chang, W. Zhao, D. Y. Kim, H. Zhang, B. A. Assaf, D. Heiman, S.-C. Zhang, C. Liu, M. H. Chan, and J. S. Moodera, *Nat. Mater.* **14**, 473 (2015).
- [18] S. Raghu, S. B. Chung, X.-L. Qi, and S.-C. Zhang, *Phys. Rev. Lett.* **104**, 116401 (2010).
- [19] R. E. V. Profumo, R. Asgari, M. Polini, and A. H. MacDonald, *Phys. Rev. B* **85**, 085443 (2012).
- [20] P. Di Pietro, M. Ortolani, O. Limaj, A. Di Gaspare, V. Giliberti, F. Giorgianni, M. Brahlek, N. Bansal, N. Koirala, S. Oh, P. Calvani, and S. Lupi, *Nat Nano* **8**, 556 (2013).
- [21] J.-Y. Ou, J.-K. So, G. Adamo, A. Sulaev, L. Wang, and N. I. Zheludev, *Nat. Commun.* **5** (2014).
- [22] A. Politano, V. M. Silkin, I. A. Nechaev, M. S. Vitiello, L. Viti, Z. S. Aliev, M. B. Babanly, G. Chiarello, P. M. Echenique, and E. V. Chulkov, *Phys. Rev. Lett.* **115**, 216802 (2015).
- [23] A. Kogar, S. Vig, A. Thaler, M. H. Wong, Y. Xiao, D. Reig-i Plessis, G. Y. Cho, T. Valla, Z. Pan, J. Schneeloch, R. Zhong, G. D. Gu, T. L. Hughes, G. J. MacDougall, T.-C. Chiang, and P. Abbamonte, *Phys. Rev. Lett.* **115**, 257402 (2015).
- [24] Y. D. Glinka, S. Babakiray, T. A. Johnson, M. B. Holcomb, and D. Lederman, *Nat. Commun.* **7**, 13054 (2016).
- [25] A. Mahoney, J. Colless, L. Peeters, S. Pauka, E. Fox, X. Kou, L. Pan, K. Wang, D. Goldhaber-Gordon, and D. Reilly, arXiv:1703.03122 [cond-mat.mes-hall].
- [26] X. Jia, S. Zhang, R. Sankar, F.-C. Chou, W. Wang, K. Kempa, E. W. Plummer, J. Zhang, X. Zhu, and J. Guo, *Phys. Rev. Lett.* **119**, 136805 (2017).
- [27] B. Ferguson and X.-C. Zhang, *Nat Mater* **1**, 26 (2002).
- [28] M. Tonouchi, *Nat Photon* **1**, 97 (2007).
- [29] R. Soref, *Nat Photon* **4**, 495 (2010).
- [30] H.-Z. Lu, A. Zhao, and S.-Q. Shen, *Phys. Rev. Lett.* **111**, 166802 (2013).
- [31] H. Zhang, C.-X. Liu, X.-L. Qi, X. Dai, Z. Fang, and S.-C. Zhang, *Nat. Phys.* **5**, 438 (2009).
- [32] W.-Y. Shan, H.-Z. Lu, and S.-Q. Shen, *New Journal of Physics* **12**, 043048 (2010).
- [33] See Supplemental Material for the derivation of the non-interacting polarization function in Eq. (4) in the main text, which includes Ref. [2].
- [34] A. Grigorenko, M. Polini, and K. Novoselov, *Nat. Photon.* **6**, 749 (2012).
- [35] G. Goldstein, C. Aron, and C. Chamon, *Phys. Rev. B* **92**, 020504 (2015).
- [36] T. Cao, Z. Li, and S. G. Louie, *Phys. Rev. Lett.* **114**, 236602 (2015).
- [37] In some literatures, a sign change of mass in the Dirac fermions with a constant mass is also called the band

- inversion [38]. However, it only exchanges the parity of wave functions but does not lead to any enhancement of the interband correlation or the Van Hove singularity. Thus, this case is not the key focus of the present paper.
- [38] S.-Q. Shen, *Topological Insulators* (Springer-Verlag, Berlin, 2012).
- [39] X.-F. Wang and T. Chakraborty, Phys. Rev. B **75**, 033408 (2007).
- [40] P. K. Pyatkovskiy, J. Phys.: Condens. Matter **21**, 025506 (2009).
- [41] A. Scholz, T. Stauber, and J. Schliemann, Phys. Rev. B **86**, 195424 (2012).
- [42] H.-R. Chang, J. Zhou, H. Zhang, and Y. Yao, Phys. Rev. B **89**, 201411 (2014).
- [43] C. J. Tabert and E. J. Nicol, Phys. Rev. B **89**, 195410 (2014).
- [44] C. Liu, T. L. Hughes, X.-L. Qi, K. Wang, and S.-C. Zhang, Phys. Rev. Lett. **100**, 236601 (2008).
- [45] We utilize the rigid-band approximation, in which the energy band structure is assumed not be changed by a slightly doping except a shift of the Fermi level. In this work, we focus on the n-doped case, namely, the Fermi level crosses the conduction bands. The p-doped case can be calculated in a similar way.

SUPPLEMENTARY MATERIAL FOR “TUNABLE INTRINSIC PLASMONS DUE TO BAND INVERSION IN TOPOLOGICAL MATERIALS”

This supplemental material contains a detailed derivation of Eq. (4) in the main text. We start with the polarization function within the one-loop approximation at a finite temperature T

$$\Pi(\mathbf{q}, i\omega_m) = k_B T \sum_{n=-\infty}^{+\infty} \frac{1}{L^2} \sum_{\mathbf{k}} \text{tr} [G(\mathbf{k}, i\Omega_n) G(\mathbf{k}', i\Omega_n + i\omega_m)], \quad (7)$$

where $\omega_m = 2m\pi k_B T$ and $\Omega_n = (2n+1)\pi k_B T$ are Matsubara frequencies, L^2 is the area of a 2D system, and $\mathbf{k}' = \mathbf{k} + \mathbf{q}$. Using the Matsubara Green's function in the eigenstate basis,

$$G(\mathbf{k}, i\Omega_n) = \sum_{\lambda} \frac{|\lambda\mathbf{k}\rangle \langle \lambda\mathbf{k}|}{i\Omega_n - E_{\lambda\mathbf{k}} + \mu}, \quad (8)$$

with μ being the chemical potential and $H(\mathbf{k})|\lambda\mathbf{k}\rangle = E_{\lambda\mathbf{k}}|\lambda\mathbf{k}\rangle$, one gets

$$\Pi(\mathbf{q}, i\omega_m) = k_B T \sum_{n=-\infty}^{+\infty} \sum_{\lambda, \lambda'} \frac{1}{L^2} \sum_{\mathbf{k}} \sum_{s, \mathbf{p}} \langle s\mathbf{p}| \frac{|\lambda\mathbf{k}\rangle \langle \lambda\mathbf{k}|}{i\Omega_n - E_{\lambda\mathbf{k}} + \mu} \cdot \frac{|\lambda'\mathbf{k}'\rangle \langle \lambda'\mathbf{k}'|}{i\Omega_n + i\omega_m - E_{\lambda'\mathbf{k}'} + \mu} |s\mathbf{p}\rangle. \quad (9)$$

After making use of the orthogonal relation $\langle \lambda\mathbf{k}|s\mathbf{p}\rangle = \delta_{\lambda s} \delta_{\mathbf{k}\mathbf{p}}$ and summing over s and \mathbf{p} , one has

$$\Pi(\mathbf{q}, i\omega_m) = k_B T \sum_{n=-\infty}^{+\infty} \sum_{\lambda, \lambda'} \frac{1}{L^2} \sum_{\mathbf{k}} \frac{1}{i\Omega_n - E_{\lambda\mathbf{k}} + \mu} \cdot \frac{1}{i\Omega_n + i\omega_m - E_{\lambda'\mathbf{k}'} + \mu} |\langle \lambda\mathbf{k}|\lambda'\mathbf{k}'\rangle|^2. \quad (10)$$

By use of the summation formula [2],

$$k_B T \sum_{n=-\infty}^{+\infty} \frac{1}{i\Omega_n - (x_1 - \mu)} \cdot \frac{1}{i\Omega_n + i\omega_m - (x_2 - \mu)} = \frac{f(x_1) - f(x_2)}{i\omega_m + x_1 - x_2}, \quad (11)$$

performing the summation over n leads to

$$\Pi(\mathbf{q}, i\omega_m) = \sum_{\lambda, \lambda'} \frac{1}{L^2} \sum_{\mathbf{k}} \frac{f(E_{\lambda\mathbf{k}}) - f(E_{\lambda'\mathbf{k}'})}{i\omega_m + E_{\lambda\mathbf{k}} - E_{\lambda'\mathbf{k}'}} |\langle \lambda\mathbf{k}|\lambda'\mathbf{k}'\rangle|^2. \quad (12)$$

Carrying out the analytic continuation from Matsubara frequencies $i\omega_m \rightarrow \omega + i\eta$, one obtains the retarded noninteracting polarization function

$$\Pi(\mathbf{q}, \omega) = \sum_{\lambda, \lambda'} \frac{1}{L^2} \sum_{\mathbf{k}} \frac{f(E_{\lambda\mathbf{k}}) - f(E_{\lambda'\mathbf{k}'})}{\omega + E_{\lambda\mathbf{k}} - E_{\lambda'\mathbf{k}'} + i\eta} |\langle \lambda\mathbf{k}|\lambda'\mathbf{k}'\rangle|^2. \quad (13)$$

Replacing $(1/L^2) \sum_{\mathbf{k}}$ with $\int \frac{d^2\mathbf{k}}{(2\pi)^2}$, one immediately reaches

$$\Pi(\mathbf{q}, \omega) = \sum_{\lambda, \lambda'} \int \frac{d^2\mathbf{k}}{(2\pi)^2} \frac{[f(E_{\lambda\mathbf{k}}) - f(E_{\lambda'\mathbf{k}'})]}{\omega + E_{\lambda\mathbf{k}} - E_{\lambda'\mathbf{k}'} + i\eta} |\langle \lambda\mathbf{k}|\lambda'\mathbf{k}'\rangle|^2, \quad (14)$$

which is the noninteracting polarization function in Eq. (4) in the main text.